Chain morphology, swelling exponent, persistence length, like-charge attraction, and charge distribution around a chain in polyelectrolyte solutions: effects of salt concentration and ion size studied by molecular dynamics simulations

Pai-Yi Hsiao*

Department of Engineering and System Science,

National Tsing Hua University, Hsinchu, Taiwan 300, R.O.C.

(Dated: February 6, 2008)

Abstract

Properties of polyelectrolytes in tetravalent salt solutions are intensively investigated by a coarse-grained model. The concentration of salt and the size of tetravalent counterions are found playing a decisive role on chain properties. If the size of tetravalent counterions is compatible with the one of monomers, the chains show extended structures at low and at high salt concentrations, whereas at intermediate salt concentrations, they acquire compact and prolate structures. The swelling exponent of a chain against salt concentration behaves in an analogous way as the morphological quantities. Under certain condition, the electrostatics gives a negative contribution to the persistence length, in companion with a salt-induced mechanical instability of polyelectrolytes. Nearly at the same moment, it appears like-charge attraction between chains. The equal size of the tetravalent ions and the monomers is the optimal condition to attain the strongest attraction between chains and the most compact chain structure. Moreover, the ions form a multi-layer organization around a chain and, thus, the integrated charge distribution reveals an oscillatory behavior. The results suggest that charge inversion has no direct connection with redissolution of polyelectrolytes at high salt concentrations.

PACS numbers:

*Electronic address: pyhsiao@ess.nthu.edu.tw

I. INTRODUCTION

Solutions of highly-charged polyelectrolytes, such as biopolymers (DNA, proteins, *etc.*) and many synthetic polyelectrolytes, exhibit striking phenomena while multivalent salts or charged molecules are added into the solutions [1–4]. If the concentration of the added salt lies within a window of concentration, the solution is separated in two phases: one is a viscous phase containing condensed or precipitated polyelectrolytes, and the other is a dilute phase in which polyelectrolytes are dissolved. If it lies outside the window, the solution is in a homogeneous phase. These phenomena are called "reentrant condensation" [5], or commonly referred as "DNA condensation" in the fields of biology and medicine [6]. This topic has attracted much attention recently due to its potential application in developing nonviral vectors of DNA for the purpose of gene therapy [7]. The amount of salt which results in the phase separation is determined by many factors, such as valence of salt, temperature, chain structure, and concentration of polyelectrolytes [2–4, 8]. It is known that the lower boundary of the window depends linearly on the concentration of polyelectrolytes but the upper one of the window is insensitive to it and roughly a constant. Both flexible polyelectrolytes and stiff polyelectrolytes display similar phase diagrams [3, 4, 9].

Despite decades of effort, our understanding on polyelectrolytes is still limited and many issues, including the reentrant condensation, are far from being resolved [10]. The aim of this paper is to investigate the properties of polyelectrolytes in salt solutions by means of computer simulations. There have been many simulations devoted to the study of polyelectrolytes [11–23]. However, most of them investigated the properties in salt-free solutions [11–16]. Only recently, due to the progress of computing power, large-scale simulations for systems with added salt can be realized. The works included, for example, flexible chains in monovalent or multivalent salt solutions [17–20], semiflexible chains with multivalent salt or charged molecules [21, 22], and rigid chains in the presence of multivalent salts [23]. But the salt concentration or the salt valence was not large enough to observe any significant evidence being able to connect to the redissolution of polyelectrolytes. Therefore, the reentrant condensation could not be discussed thoroughly in these works. Allahyrarov *et al.* [24] recently studied the effective interaction between two immobile DNAs in the presence of tetravalent counterions. They have found that the effective interaction yields an attractive minimum at short distances which then disappears in favor of a shallow minimum at

large separations, indicating the occurrence of DNA condensation and redissolution and a novel stable mesocrystal. In a more recent study [25], we have investigated the properties of mobile polyelectrolytes in tetravalent salt solutions and demonstrated that following a collapsed transition, polyelectrolytes undergo reexpanding transition upon addition of the salt. This phenomenon is just a single-chain version of the condensation and the redissolution of polyelectrolytes. Moreover, by varying the ion size, we have shown that the excluded volume of ions plays a decisive role on the reentrant condensation. However, to well understand the phenomena, there is still a far way to go. For example, is it possible to obtain any information related to the phase boundary of reentrant condensation from simulations? There exist theories to explain the phase boundary [3–5] but it has never been studied in simulations. Concerning the size of polyelectrolyte in multivalent salts, Muthukumar and coworkers have applied single and double screening theories to explain the collapsed transition of chains [18, 26, 27]. However, no existing theory can predict chain reexpansion in the region of high salt concentration. Moreover, chain morphology is essential to understand the properties of polyelectrolytes. It can be described by many quantities, such as asphericity and prolateness parameter [28]. To our knowledge, no such study has been reported yet for strongly-charged polyelectrolytes. An alternative way to understand polymers is to study scaling behavior. Although the concept of scaling has been successfully applied to neutral polymers [29], application of this concept to polyelectrolytes [30–33] has encountered many difficulties owing to the long-range nature of Coulomb interaction. In this paper, we compute the single-chain structure factor. The swelling exponent is then calculated by studying the power-law-like regime of the structure factor. Since properties of polyelectrolytes depend strongly on ion size, we investigate in this paper the effect of ion size too. In our previous work [25], the sizes of ions were set to identical and varied simultaneously. As a consequence, Bjerrum association [34] was strongly intervened, particularly when ions were small. This setup has a disadvantage that the system was easily jammed by large ions, leading to the impossibility of investigation of the cases of big ions. Therefore, in this study we vary only the size of the multivalent counterions and fix unchanged the one of the other ions, so that the ion size effect is restrictedly investigated.

In the study of polyelectrolytes, it is tempting to discuss the long range nature of Coulomb interaction using the concept of electrostatic persistence length. Odijk [35], Skolnick and Fixman [36] predicted that the electrostatic persistence length is proportional to the square

of the screening length r_s. The deduction was based upon Debye-Hückel theory. Consequently, the effective intramolecular interaction is always repulsive, resulting in a positive electrostatic persistence length [37, 38]. However, experiments have shown that electrostatic persistence length can be negative under certain condition so that electrostatics gives a reversed contribution to chain flexibility [39, 40]. Simulations on this issue [41–45] were mainly performed within Debye-Hückel approximation using a screened Coulomb potential $U_{\rm DH}(r) \propto e^{-r/r_s}/r$ to describe the screening effect of salt without involving explicitly salt ions. A negative electrostatic persistence length, hence, has never been reproduced in the simulations. Noticeably, it is known that linear screening theory is valid only for a weakly-charged system and breaks down for a highly-charged one, such as DNA and many biopolymers, due to strong ion correlations [17, 46, 47]. Recently, by employing a loop expansion method which goes beyond mean field, Ariel and Andelman were able to predict the negative regime of the electrostatic persistence length for a strongly-charged rodlike polyelectrolyte [48]. Therefore, we expect that to observe a negative electrostatic persistence length, one should incorporate salt ions explicitly and use the bare Coulomb potential in simulations. Our study fulfills this requirement and hence offer a good chance to verify the above phenomenon and theory.

Charge inversion is a universal phenomenon, occurred when a strongly charged macroion binds so many counterions that its net charge alters sign [49]. Nguyen *et al.* intended to link charge inversion with the reentrant condensation of polyelectrolytes [5]. The idea was based upon that counterions form strongly correlated liquid on the surface of polyelectrolytes. In an intermediate salt region, the bare charges of the chains are almost neutralized by the condensed counterions; the correlation-induced attraction results in the condensation of polyelectrolytes. In a high-salt region, the counterions overcompensate the chain bare charges; Coulomb repulsion between chains dominates the attraction and, in consequence, the condensates are redissolved into the solution. Solis and Olvera de la Cruz gave a different point of view using a theory called "two-state model" [50, 51]. They predicted that charge inversion is not necessarily occurred with redissolution of polyelectrolytes. Although overcompensated by counterions, the redissolved polyelectrolytes can have either sign due to the association of coions [52]. This association depends strongly on the ion size which was not considered in the study of Nguyen *et al.* [5]. Therefore, Solis and Olvera de la Cruz predicted a charge distribution which oscillates from a polyelectrolyte, in accordance with the

profile observed in our previous work [25]. In this paper, we investigate more extreme cases, including much smaller and much larger ions. We also study like-charge attraction between chains by calculating the potential of mean force and determine the conditions under which the attraction takes place.

The rest of the article is organized as follows. Model and simulation details are given in Sec. II. Results are discussed in Sec. III. It is divided into five subsections. The first subsection (Sec. III A) is devoted to the study of the radius of gyration of a polyelectrolyte where salt concentration and polyelectrolyte concentration are varied. The results provide information helpful in understanding the boundaries of the condensation window. Sec. III B studies the morphology of multiple polyelectrolytes in salt solutions. We compute several quantities, including shape factors, asphericity, and prolateness parameter. The effect of size of multivalent ions is discussed. Single-chain structure factor is, then, calculated in Sec. III C. By least-square fitting the power-law-like regime, we compute the swelling exponent of a polyelectrolyte, which provides a fundamental vision how strongly-charged polyelectrolytes scale in salt solutions. Sec. III D deals with persistence length. The negative regime of the electrostatic persistence length is successfully reproduced in the simulations. Comparison of the results with theoretical predictions is made. Sec. III E provides a general picture of the effective interaction between polyelectrolytes by computing the potential of mean force. As long as knowing the condition to appear like-charge attraction between chains and the integrated charge distribution around a chain (Sec. III F), we are able to arbitrate if the phenomena of charge inversion and the redissolution of polyelectrolytes are related. We give our conclusions in Sec. IV.

II. MODEL AND SIMULATION METHOD

We employed a coarse-grained model to simulate a polyelectrolyte system. The system contains four bead-spring chains, one of which is composed of 48 beads (monomers). Each monomer dissociates a monovalent cation (counterion) into a solution and carries a negative unit charge. There are totally 192 monovalent cations in the solution. Solvent molecules are not modeled explicitly. Their effect is taken into account implicitly by considering them as a medium of constant dielectric constant. The geometry of the medium is cubic and periodic boundary condition is applied to simulate bulk environment. Salt molecules are

added into the system. In the solution, they are dissociated into cations (counterions) and anions (coions). We assume that the cations are tetravalent and the anions are monovalent. The amount of the cations and anions obeys the condition of charge neutrality.

Three types of interactions are included in our simulations. The first one is the excluded volume interaction described by a purely repulsive Lennard-Jones (LJ) potential,

$$U_{\mathrm{LJ}}(r) = \begin{cases} 4\varepsilon_{\mathrm{LJ}}\left[(\sigma/r)^{12} - (\sigma/r)^{6}\right] + \varepsilon_{\mathrm{LJ}} & \text{for } r \le \sqrt[6]{2}\sigma \\ 0 & \text{for } r > \sqrt[6]{2}\sigma \end{cases} , \tag{1}$$

where r is the distance between two particles, $\varepsilon_{\mathrm{LJ}}$ is the interaction strength, and σ is the collision diameter. We assume that all the particles have identical $\varepsilon_{\mathrm{LJ}}$ but the collision diameter may be different. The collision diameters for monomer, monovalent cation, tetravalent cation, and anion are denoted by σ_{m}, σ_{+1}, σ_{+4}, and σ_{-1}, respectively. Lorentz-Berthelot mixing rule [53] is applied for the interaction between different kinds of particles.

The second interaction is called finitely extensible nonlinear elastic (FENE) potential [54] and used to describe the bond connection between adjacent monomers on a chain. It reads as

$$U_{\mathrm{FENE}}(\ell) = -\frac{1}{2}k_{\mathrm{FENE}}R_0^2 \ln\left(1 - \frac{\ell^2}{R_0^2}\right) , \tag{2}$$

where k_{FENE} is the spring constant, ℓ is bond length, and R_0 is the maximum extension of a bond. All particles interact via the third interaction, Coulomb interaction, which is written as

$$U_{\mathrm{coul}}(r) = k_{\mathrm{B}}T\ell_{\mathrm{B}}\frac{Z_i Z_j}{r} \tag{3}$$

where $Z_i e$ is the charge of the ith particle, T is the temperature, k_{B} is the Boltzmann constant, and ℓ_{B} is the Bjerrum length defined as the separation distance at which the Coulomb potential between two unit charges e equals to the thermal energy $k_{\mathrm{B}}T$. ℓ_{B} is equal to $e^2/(4\pi\epsilon\epsilon_0 k_{\mathrm{B}}T)$ where ϵ is the dielectric constant and ϵ_0 is the vacuum permittivity.

We perform molecular dynamics (MD) simulations in this study [75]. We set σ_{+1} and σ_{-1} equal to σ_{m} and vary the size of tetravalent cation σ_{+4} from $0.0\sigma_{\mathrm{m}}$ to $4.0\sigma_{\mathrm{m}}$ to investigate the effect of ion size on properties of the polyelectrolyte solution. Simulation parameters are chosen as follows: $\varepsilon_{\mathrm{LJ}} = 0.8333k_{\mathrm{B}}T$, $k_{\mathrm{FENE}} = 5.8333k_{\mathrm{B}}T/\sigma_{\mathrm{m}}^2$, and $R_0 = 2\sigma_{\mathrm{m}}$. The Bjerrum length is set to $\ell_{\mathrm{B}} = 3\sigma_{\mathrm{m}}$. Similar systems in salt-free solutions have been investigated by Stevens and Kremer [14]. We assume that the masses of all the particles are identical and equal to m, and choose σ_{m} and $k_{\mathrm{B}}T$ to be the length unit and the energy unit, respectively.

Therefore, the natural time unit is $\tau = \sigma_{\rm m}\sqrt{m/(k_{\rm B}T)}$. The system is studied in canonical ensemble where the temperature is controlled using Nosé-Hoover thermostat with the frequency of heat transfer with thermostat equal to $1.0\tau^{-1}$. Coulomb interaction is calculated by the technique of Ewald sum. Except in Sec. III A, the monomer concentration is fixed at $C_{\rm m} = 0.008\sigma_{\rm m}^{-3}$ which corresponds to a box size $L = 28.8\sigma_{\rm m}$, whereas the salt concentration is varied. The amount of salt is controlled such that the volume fraction of total particles is smaller than 30%. Equations of motion are integrated applying Verlet algorithm where time step is set to 0.005τ. Each simulation starts with an equilibration phase of 2×10^6 MD steps and is followed by a production run of 10^7 MD steps in which data are collected every 1000 steps. In order to shorten the notation, we will use $\sigma_{\rm m}$ as the length unit, $\sigma_{\rm m}^{-3}$ as the concentration unit , and e as the charge unit in the following text.

III. RESULTS AND DISCUSSIONS

A. Radius of gyration of a polyelectrolyte at different monomer concentrations

We started our study by simulating a single polyelectrolyte with added tetravalent salt at various monomer concentrations. The chain consists of 48 monomers and the size of the tetravalent cations is set to be identical to the one of the monomers. We used the radius of gyration to characterize the chain size. The radius of gyration $R_{\rm g}$ is calculated by the equation

$$R_{\rm g}^2 = \frac{1}{N}\sum_{i=1}^{N}(\vec{r}_i - \vec{r}_{\rm cm})^2 \tag{4}$$

where N is the number of monomers on the chain, $\vec{r}_i$ is the position vector of the ith monomer, and $\vec{r}_{\rm cm}$ the center of mass of the chain. The results are presented in Fig. 1 where the mean square radius of gyration $\langle R_{\rm g}^2 \rangle$ is plotted as a function of salt concentration $C_{\rm s}$ at four monomer concentrations, $C_{\rm m} = 0.00032$, 0.002, 0.008 and 0.016. The angular bracket $\langle \cdot \rangle$ means averaging over chain configurations. Two behaviors were observed. The first one is that each curve displays a similar trend of behavior against salt concentration. Upon addition of salt, the chain undergoes two structural transitions: a collapsed transition and a followed reexpanding transition, as having been observed in the previous work [25]. The first transition results from the screening of the Coulomb interaction by the added salt. The second transition is still not well understood although it is a result of the competition between

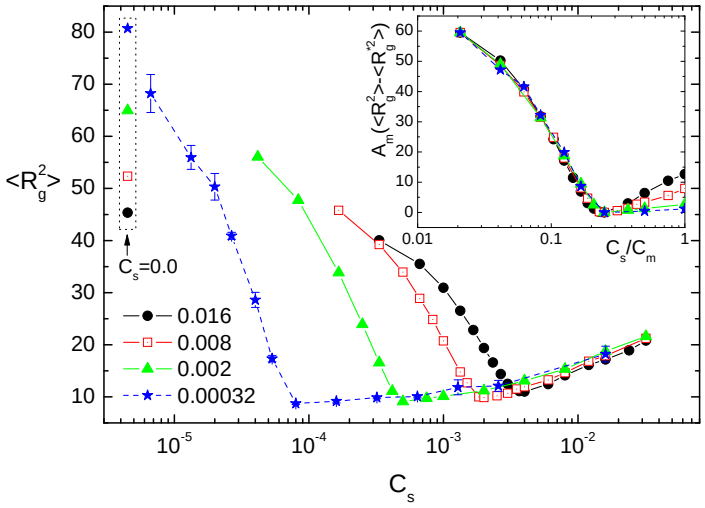

FIG. 1: $\langle R_{\rm g}^2\rangle$ as a function of $C_{\rm s}$ at four monomer concentrations, $C_{\rm m}$ = 0.00032, 0.002, 0.008, and 0.016. The symbols used to represent the four $C_{\rm m}$ are indicated at the left-bottom side of the figure. The value of $\langle R_{\rm g}^2\rangle$ in a salt-free solution ($C_{\rm s}$=0.0) is depicted near the left vertical axis. The four curves in the regime $C_{\rm s} \leq C_{\rm s}^*$ can overlap each other (shown in the inset) under a suitable transformation described in the text.

energetic gain and entropic loose in counterion condensation and in shape transformation of polyelectrolytes to minimize the free energy. We observed that the minimum of $\langle R_{\rm g}^2\rangle$ appears near the salt concentration $C_{\rm s}^* = C_{\rm m}/4$ and the more dilute the monomer concentration, the smaller value the minimum of $\langle R_{\rm g}^2\rangle$ will be. $C_{\rm s}^*$ is the equivalence point at which the amount of charges of the tetravalent counterions exactly neutralizes the charges on polyelectrolytes as if the salts and the polyelectrolytes are in the stoichiometric reaction. We will call $C_{\rm s}^*$ the equivalence concentration. In a salt-free solution ($C_{\rm s} = 0$), we found that the chain size increases with decreasing monomer concentration (refer to the four data points near the left vertical axis of the figure). This effect has been discussed in literatures [14, 33] and our results are in accordance with them. And the second behavior is that $\langle R_{\rm g}^2\rangle$ for different $C_{\rm m}$ attains approximately the same value while the salt concentration is larger than the equivalence concentration. Therefore, the curves approximately overlap each other. We noticed, furthermore, that in the region $C_{\rm s} \leq C_{\rm s}^*$, the $\langle R_{\rm g}^2\rangle$ curves for different $C_{\rm m}$ can also lie over each other under an appropriate transformation. We demonstrate this overlap in the inset of Fig. 1 where the abscissa is $C_{\rm s}/C_{\rm m}$ and the ordinate is $A_{\rm m}(\langle R_{\rm g}^2\rangle - \langle R_{\rm g}^{*2}\rangle)$ with $\langle R_{\rm g}^{*2}\rangle$ the minimum value of $\langle R_{\rm g}^2\rangle$. $A_{\rm m}$ depends smoothly on $C_{\rm m}$ and, in the figure, is equal

to 1, 1.267, 1.657, and 2.049 for $C_{\rm m} = 0.00032$, 0.002, 0.008, and 0.016, respectively.

The size of polyelectrolytes in multivalent salt solutions has been studied by small-angle scattering experiments [55]. The results showed that it diminishes with increasing or decreasing $C_{\rm s}$ toward the region where the condensation of polyelectrolytes occurs (cf. Table 2 of Ref. [55]). The results of our simulations are in accordance with the experiments. We make a hypothesis that chain size can be served as a qualitative condition to distinguish between a monophasic solution of polyelectrolyte and a diphasic one. More precisely, if the chain size is larger than some value, the chains are dissolved in the solution and the system is in a homogeneous phase; if it is smaller, the chains are precipitated from the solution and a phase separation occurs. Under this hypothesis, polyelectrolyte solutions of different $C_{\rm m}$ become monophasic as C_s is increased over a concentration in the high-salt region, since the chain size exceeds the some value nearly at the same $C_{\rm s}$ due to the similarity of the $\langle R_{\rm g}^2 \rangle$ curves against $C_{\rm s}$ in this region. Therefore, the upper boundary of the salt concentration window for the condensation of polyelectrolyte is independent of $C_{\rm m}$. Similarly, the lower boundary of the window approximately depends linearly on $C_{\rm m}$, owing to the similarity of the $A_{\rm m}(\langle R_{\rm g}^2 \rangle - \langle R_{\rm g}^{*2} \rangle)$ curves against $C_{\rm s}/C_{\rm m}$ in the low-salt region; the weak dependence of $A_{\rm m}$ and $\langle R_{\rm g}^{*2} \rangle$ on $C_{\rm m}$ ensures that the chain size surpasses the some value roughly at the same $C_{\rm s}/C_{\rm m}$. Therefore, Fig. 1 provides an essential information to understand the boundaries of reentrant condensation.

The aim of this article is to understand the properties of multiple flexible polyelectrolytes with added salt in an aqueous solution. It is known that the Bjerrum length $\ell_{\rm B}$ in water is equal to 7.14Å at room temperature. Our simulation setup, hence, corresponds to a collision diameter $\sigma_{\rm m}$ of monomer equal to 2.38Å. This model represents a polyelectrolyte system with linear charge density equal to a unit charge per 2.62Å[76], and can be employed to simulate a strongly-charged system such as sodium polystyrene sulfonate. The four monomer concentrations studied in this section, while converted to real unit, are equal to 0.039M, 0.246M, 0.986M, and 1.971M, respectively. Even the largest $C_{\rm m}$ is still smaller than the overlap threshold $C_{\rm m}^*$ estimated by $3N/(4\pi R_{\rm g}^3)$. Therefore, our systems are dilute polymer solutions. Readers should be aware that the value up to nearly 2M is a very high monomer concentration for a real polymer system, and our systems are *dilute* only in the formal meaning of the world since the chains are very short. In the following sections, we fix $C_{\rm m}$ at 0.008 and simulate a system comprising multiple chains. This monomer concentration

is one or two order of magnitude higher than a typical monomer concentration used in experiments [3, 4, 55]. However, based on the fact that systems at different monomer concentrations reveal similar evolution of chain size against salt concentration, the results obtained at $C_{\rm m} = 0.008$ can be used to understand a system at more dilute $C_{\rm m}$. We mention that this $C_{\rm m}$ is a choice so that the simulation box is not so big. Therefore, the amount of the added salt is controllable under limited computing resources. Consequently, to study the behavior of polyelectrolytes in salt solutions, covering a broad range of salt concentration, becomes numerically feasible.

B. Shape of polyelectrolytes

In this section and in the followings, the studied system contains four polyelectrolytes and the monomer concentration is fixed at $C_{\rm m} = 0.008$. This section is devoted to the study of chain conformation in tetravalent salt solutions. The effects of salt concentration and size of tetravalent counterions are investigated. We vary the size of tetravalent counterion, σ_{+4}, from 0.0 to 4.0 and fix the size of the other ions at 1.0. A large σ_{+4} can represent a large cation, a large ion group, or a large charged colloid. It can be also a result of the hydration of a small ion. A small σ_{+4} may be less representative for real systems but theorists are generally interested in it because many models are established on the base of vanishing ion size.

Morphology of a polymer can be quantified by many quantities. The first quantity that we studied is the shape factor η, defined as the ratio of the mean-square end-to-end distance, $\langle R_{\rm e}^2 \rangle = \langle (\vec{r}_1 - \vec{r}_N)^2 \rangle$, to the mean-square radius of gyration $\langle R_{\rm g}^2 \rangle$. η attains a value 12 for a rodlike polymer, 6.3 for a flexible chain in a good solvent, and 6 for an ideal chain [14]. For a compact structure, the value of η is small. For example, if the chain has a spherical morphology and the two ends are randomly positioned, η is equal to 2. In Fig.2(a), we show how the shape factor η varies with $C_{\rm s}$ at different σ_{+4}. In the figure, a reference curve, marked by "neutral", is depicted. It represents a system composed of four neutral polymers of 48 monomers in tetravalent salt ($\sigma_{+4} = 1.0$) solutions. Focus firstly on the polyelectrolyte solutions with $\sigma_{+4} = 1.0$, 1.4 and 2.0. We witnessed that η decreases at first and then increases upon addition of salt, in analogy of the radius of gyration studied in the previous section, and shows a V-shaped curve against $C_{\rm s}$ in the semilog plot. In the low-salt

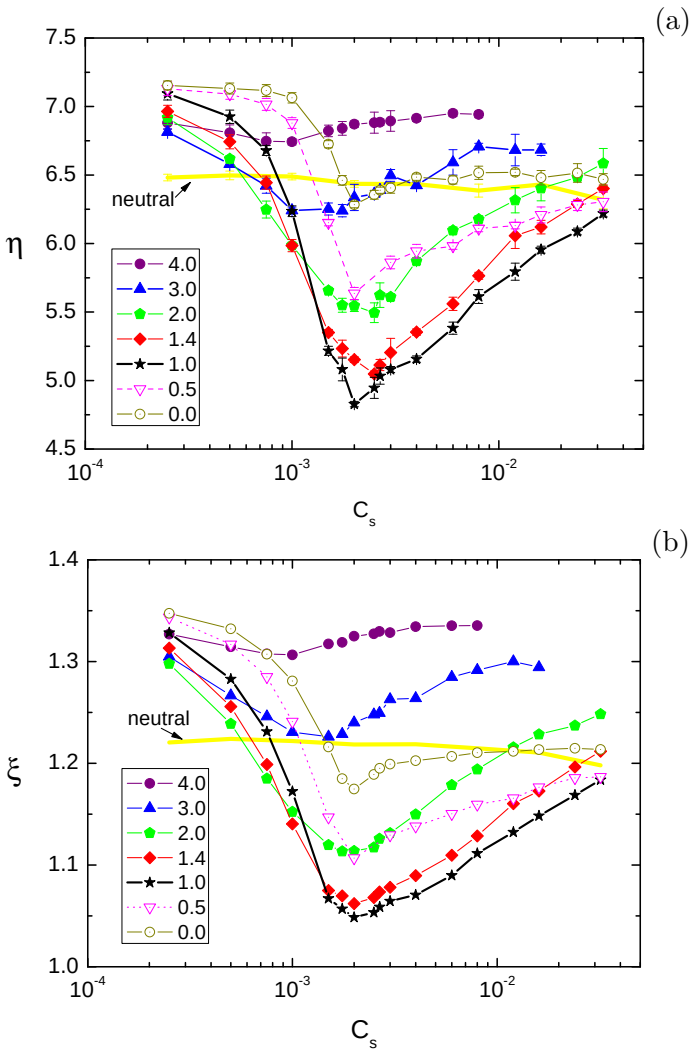

FIG. 2: (a) $\eta \equiv \langle R_{\rm e}^2\rangle/\langle R_{\rm g}^2\rangle$ as a function of $C_{\rm s}$, and (b) $\xi \equiv \langle R_{\rm g}^2\rangle^{1/2}/\langle R_{\rm h}\rangle$ as a function of $C_{\rm s}$, for the cases of different size σ_{+4} of the tetravalent counterions. The symbol used for each σ_{+4} is indicated at the left-bottom side of the figures. The error bars are smaller than the size of the symbols. The result for neutral polymers is depicted as reference and marked by "neutral".

region or in the high-salt region, η is larger than or close to the value 6.3, indicating that the chains have elongated or coil-like structures. In between, it appears a minimum near the equivalence concentration $C_{\rm s}^* = 0.002$. The value of η tells us that the chains possess compact structures but not so compact as spheres. For the cases with larger σ_{+4} ($\sigma_{+4} = 3.0$ and 4.0), η shows a shallow minimum and the whole curve stays basically above the value 6.3. In these cases, the chains are in an extended state. It is worth to notice that for $\sigma_{+4} \geq 1.0$, η, in principle, increases with σ_{+4} at a given $C_{\rm s}$. Now pay attention to the cases

with $\sigma_{+4} < 1.0$. η displays a similar V-shaped curve against C_s but opposite to the previous cases, its value increases with decreasing σ_{+4}. Moreover, the degree of chain reexpansion in the high-salt region is weakened while σ_{+4} is decreased. Noticeably, for the case $\sigma_{+4} = 0.0$, η displays a sharp transition from a value 7.2 in the low-salt solution to a value 6.5 in the vicinity of C_s^*. In the latter region, the chains behave similarly to neutral polymers.

The second quantity that we studied is ξ, which is the ratio of the radius of gyration $\langle R_g^2 \rangle^{1/2}$ to the hydrodynamic radius $\langle R_h \rangle$ computed by $R_h^{-1} = N^{-2}(\sum_{i=1}^{N} \sum_{j=1, j\neq i}^{N} r_{ij}^{-1})$. ξ is equal to $\sqrt{3/5} \simeq 0.775$ for a hard sphere and attains a value 2.25 for a rodlike chain [56]. Renormalization group theory has predicted $\xi \simeq 1.56$ in a good solvent and $\xi \simeq 1.24$ at Θ point [57], both of which have been shown in agreement with experiments [58]. We present in Fig. 2(b) the variation of ξ against C_s. The referenced curve for the system of neutral polymers is depicted. The curve was found very close to the value 1.24, which seems to indicate an ideal-chain behavior. However, the neutral chains should behave as random coils and the value of ξ would be larger than 1.24. The deviation of ξ from the value of a coil is probably due to the short chain length used in our simulations. Dünweg *et al.* have studied the finite size effect and shown that the dependence of ξ on chain length is not negligible [59]. Therefore, ξ reported here departs slightly from the asymptotic value of an infinite chain length. Nonetheless, the results are still indicative and useful to understand how ξ varies with salt concentration. In the small C_s region, the polyelectrolytes are more extended than the neutral polymers. In the middle region of C_s, the chains attain compact structures when $0.5 \leq \sigma_{+4} \leq 2.0$. The dependence of ξ upon σ_{+4} resembles to that of η. For large σ_{+4} ($\sigma_{+4} > 2.0$), the chains are elongated. For vanishing σ_{+4}, we observed that following a sharp decrease, ξ reattains approximately a constant value, close to that for the neutral polymers.

A more fundamental way to study the shape of a polymer is to investigate the tensor of radius of gyration $\mathcal{T}$ [60], defined by:

$$\mathcal{T}_{\alpha\beta} = \frac{1}{2N^2} \sum_{i=1}^{N} \sum_{j=1}^{N} (r_{i\alpha} - r_{j\alpha})(r_{i\beta} - r_{j\beta}) \tag{5}$$

where $\alpha, \beta = 1, 2, 3$ denote the three Cartesian components and $r_{i\alpha}$ is the α component of the position of the ith monomer. Let λ_1, λ_2 and λ_3 be the three eigenvalues of $\mathcal{T}$. A quantity called "asphericity" [28], which measures the deformation from a spherical geometry, is

defined by

$$A = \frac{1}{2}\left\langle \frac{(\lambda_1-\lambda_2)^2+(\lambda_2-\lambda_3)^2+(\lambda_3-\lambda_1)^2}{(\lambda_1+\lambda_2+\lambda_3)^2} \right\rangle . \tag{6}$$

It takes a value between 0 (sphere) and 1 (rod). For a coil polymer, it is 0.431 obtained from simulations [61]. Another quantity describing the degree of prolateness is defined by

$$P = \left\langle \frac{(\lambda_1-\bar{\lambda})(\lambda_2-\bar{\lambda})(\lambda_3-\bar{\lambda})}{\bar{\lambda}^3} \right\rangle \tag{7}$$

where $\bar{\lambda} = (\lambda_1+\lambda_2+\lambda_3)/3$ [28]. It is ranged from $-1/4$ to 2 and can be used to distinguish between a prolate shape ($0 < P < 2$) and an oblate one ($-\frac{1}{4} < P < 0$). For neutral polymers in the dilute limit, simulations predict a prolate chain with $P = 0.541$ [62] . We present in Figs. 3(a) and 3(b) the asphericity A and the prolateness parameter P as a function of $C_{\rm s}$. Resembling to the behaviors of η and ξ, A and P show a minimum value in the vicinity of $C_{\rm s}^*$. The curve associated to $\sigma_{+4} = 1.0$ roughly separates two different behaviors of evolution: A and P increase with increasing and with decreasing σ_{+4} from 1.0. The value of A lies between 0.275 and 0.55. Therefore, even in a compact structure (where $C_{\rm s}$ is near $C_{\rm s}^*$), the chain shape is asymmetric. In a low-salt solution, the chains show extended morphology but are not as elongated as rods. On the other hand, P is larger than zero for all of the studied cases, indicating that the polyelectrolytes display prolate conformation. At a high salt concentration, A is close to 0.45 and P is close to 0.54, suggesting once more that the polyelectrolytes behave as the neutral polymers in the high-salt region. For the case with null σ_{+4}, chain reexpansion does not occur; A and P stay at a constant value when $C_{\rm s}$ goes beyond $C_{\rm s}^*$. The results obtained in this section strongly suggest that $\sigma_{+4} = 1.0$ is the optimal condition to pack polyelectrolytes into the smallest volume.

C. Single-chain structure factor and swelling exponent

In this section, we investigate the single-chain structure factor. This quantity is experimentally accessible and provides an essential information to theoretical analysis. The single-chain structure factor is defined by

$$S(\vec{q}) = \frac{1}{N_{\rm p}N}\sum_{p=1}^{N_{\rm p}}\left\langle \left| \sum_{j=1}^{N} \exp(i\vec{q}\cdot\vec{r}_{p,j}) \right|^2 \right\rangle \tag{8}$$

where $\vec{q}$ is the scattering wavevector, $N_{\rm p} = 4$ is the number of polymer chains, $N = 48$ is the number of monomers on a chain, and $\vec{r}_{p,j}$ is the position of the jth monomer on the pth

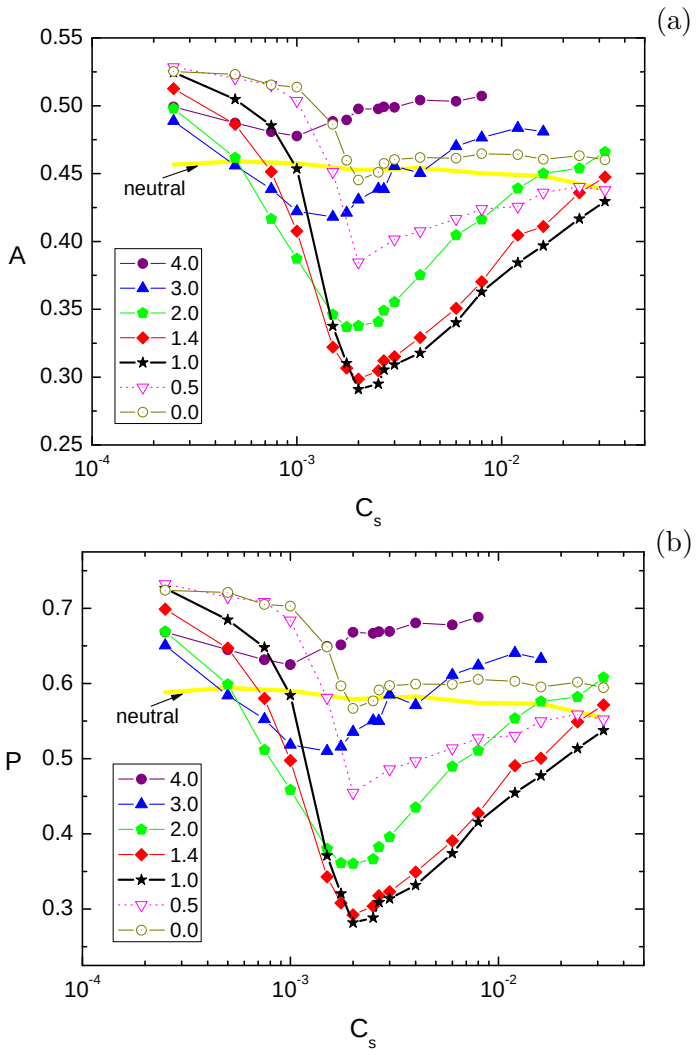

FIG. 3: (a) A as a function of $C_{\rm s}$, and (b) P as a function of $C_{\rm s}$, for different σ_{+4}. The symbol used for each σ_{+4} is indicated at the left-bottom side of the figures. The error bars are smaller than the size of the symbols. The result for neutral polymers is depicted as reference and marked by "neutral".

chain. Suppose that the system has spherical symmetry. The dependence of the structure factor on the orientation of $\vec{q}$ can be therefore integrated out: $S(q) = \frac{1}{4\pi}\int d\Omega\, S(\vec{q})$ where q is the norm of $\vec{q}$ and Ω is the solid angle. This integration was performed numerically by sampling over a set of randomly-oriented $\vec{q}$ vectors. We present, in Fig. 4(a), $S(q)$ at several salt concentrations for the case of $\sigma_{+4} = 1.0$. For the reason of clarity, the curves in the figure have been multiplied by 2^n with n being increased by one for each curve from the bottom to the top. $S(q)$ for the neutral polymers is depicted as reference with $n = 0$.

We witnessed that $S(q)$ shows typical behavior. In the Guinier regime ($qR_{\rm g} \ll 1$), $S(q)$ behaves similarly to $N(1 - q^2\langle R_{\rm g}^2\rangle/3)$. It is demonstrated by plotting $N(1 - q^2\langle R_{\rm g}^2\rangle/3)$ (in dotted curve) near the corresponding $S(q)$ with the value of $\langle R_{\rm g}^2\rangle$ adopted from Sec. III B. The dotted curve terminates at $q = R_{\rm g}^{-1}$ in order to indicate the boundary of the Guinier regime. In the regime $R_{\rm g}^{-1} \ll q \ll \sigma_{\rm m}^{-1}$, $S(q)$ shows power-law-like behavior, manifested by a linear dependence of $\log S(q)$ on $\log q$. The slope s of the linear dependence is related to the swelling exponent ν by the relation $\nu = -1/s$, which describes the size extension of a polymer: $R_{\rm g} \sim N^{\nu}$. In the regime $q > \sigma_{\rm m}^{-1}$, $S(q)$ displays non-universal behavior. However, while $q \gg \sigma_{\rm m}^{-1}$, self-scattering of monomer is the only contribution, leading, therefore, $S(q)$ to a universal value 1. We mention that the Krathy regime, in which $S(q) \sim q^{-2}$, is not observed in our study because the system is a dilute solution and the chain length is not long enough [63]. For σ_{+4} other than 1.0, we observed analogous trends of behavior. For example, the variation of $S(q)$ for different σ_{+4} at the equivalence concentration is presented in Fig. 4(b), in which we rediscovered the three regimes: the Guinier regime, the power-law-like regime and the non-universal regime. We noticed that in the last regime, a small bounce appears on the curve and, with increasing the size of tetravalent ions, gradually moves toward small q.

The swelling exponent ν of the polyelectrolytes was calculated by performing least-square fits in the log-log plot of $S(q)$ in the power-law-like regime. The fitting region was chosen to be $0.63 < q < 1$ and the fitting reliability has been verified to be excellent. We present the results of the swelling exponent ν in Fig. 5. ν for the referenced neutral polymers was verified at first and found to attain a value close to the Flory's one, 0.6. Next, we focused on the swelling exponent for the polyelectrolytes. We observed that ν exceeds the value for the neutral polymers at a low salt concentration. It indicates a strong extension of chain size due to Coulomb repulsion between monomers. For the cases with $\sigma_{+4} = 0.5$, 1,0, 1,4, and 2.0, the swelling exponent shows a V-shaped curve against $C_{\rm s}$: ν decreases and then increases with increasing salt concentration. A minimum occurs near the equivalence concentration $C_{\rm s}^*$ and, at this moment, the chains show compact structures but are less compact than spheres because a spherical structure scales as $N^{1/3}$. We remark that the swelling exponent obtained here for $\sigma_{+4} = 1.0$ is consistent with that obtained by direct variation of the chain length of a system containing a single polyelectrolyte [64] except in the mid-salt region where ν in the latter study is slightly smaller and acquires a value 1/3 at $C_{\rm s}^*$. This deviation is

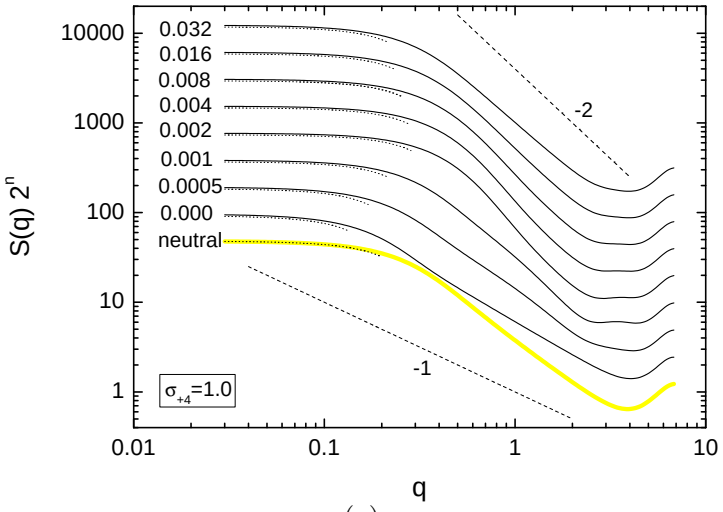

(a)

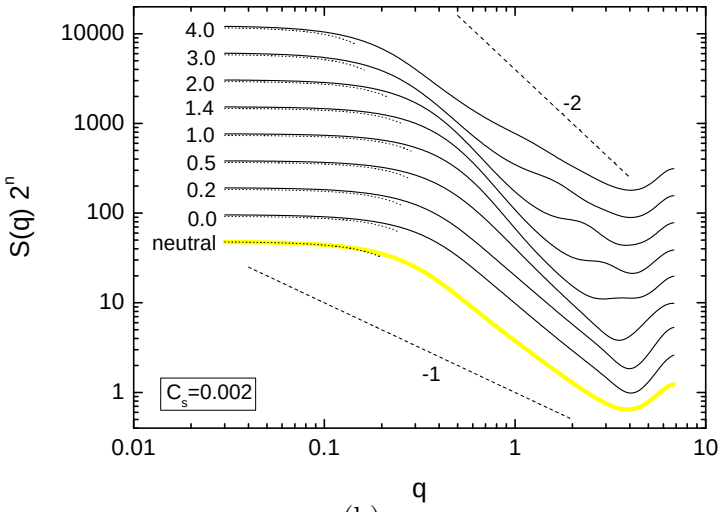

(b)

FIG. 4: (a) $S(q)$ for $\sigma_{+4} = 1.0$ at different $C_{\rm s}$ and (b) $S(q)$ at $C_{\rm s} = 0.002$ for different σ_{+4}. The value of $C_{\rm s}$ or σ_{+4}, at which the simulations were running, is indicated at the left side of each corresponding curve. $S(q)$ for the neutral polymers at $C_{\rm s} = 0.002$ is depicted as reference and marked by "neutral". For clarity, the curves, from bottom to top, have been multiplied by a factor 2^n with n started from zero and increased by one for every curve. The dotted curve, near each $S(q)$ and terminated at $q = R_{\rm g}^{-1}$, is the Guinier function $N(1 - q^2\langle R_{\rm g}^2\rangle/3)$. Two dashed lines, which represent two power-law dependences, q^{-1} and q^{-2} (marked by "-1" and "-2", respectively), are drawn in the plots.

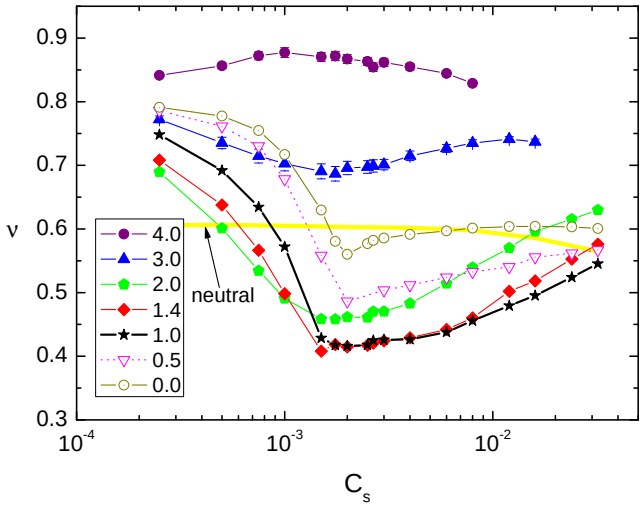

FIG. 5: ν as a function of $C_{\rm s}$ for different σ_{+4}. The symbol used for each σ_{+4} is indicated at the left-bottom side of the figure. ν for the referenced neutral-polymer system is depicted and marked by "neutral".

due to multi-chain aggregation occurred in our system, which deforms the chain shape from a sphere and, consequently, increases ν. For the case with vanishing σ_{+4}, following a drastic decrease, ν retains roughly a value 0.6 in the high-salt region and the chains, hence, scale like the neutral polymers. For the cases with large σ_{+4} (σ_{+4} = 3.0 and 4.0), ν is greater than 0.6 but still less than 1.0. The chains, hence, do not reveal rigid rod-like structures. In principle, σ_{+4} = 1.0 separates two behaviors of evolution at a salt concentration: ν increases with increasing and with decreasing σ_{+4} from 1.0. The results demonstrate again that the polyelectrolytes are mostly condensed while the size of the tetravalent counterions is compatible with the one of the monomers.

D. Persistence length

There is a considerable interest to understand the variation of the persistence length of a polyelectrolyte against salt concentration. Persistence length is a local property, which measures the stiffness of a polymer, and is distinguished from global conformational quantities. There are many ways to define the persistence length [42, 65]. In this section, we adopt a

microscopic definition to calculate it:

$$\ell_{\rm p} = \frac{1}{2b} \sum_{i=0}^{(N/2)-1} \langle \vec{b}_{N/2} \cdot \vec{b}_{(N/2)-i} + \vec{b}_{N/2} \cdot \vec{b}_{(N/2)+i} \rangle \tag{9}$$

where $\vec{b}_j = \vec{r}_{j+1} - \vec{r}_j$ is the jth bond vector and $b = \langle \vec{b}_j^2 \rangle^{1/2}$ is the root-mean-square bond length. In this definition, the contribution of the finite bond length, which corresponds to the $i = 0$ term in Eq. 9, is considered. The obtaining $\ell_{\rm p}$ as a function of $C_{\rm s}$ for different σ_{+4} is plotted in Fig. 6. Resembling to the quantities of chain conformation, $\ell_{\rm p}$ decreases

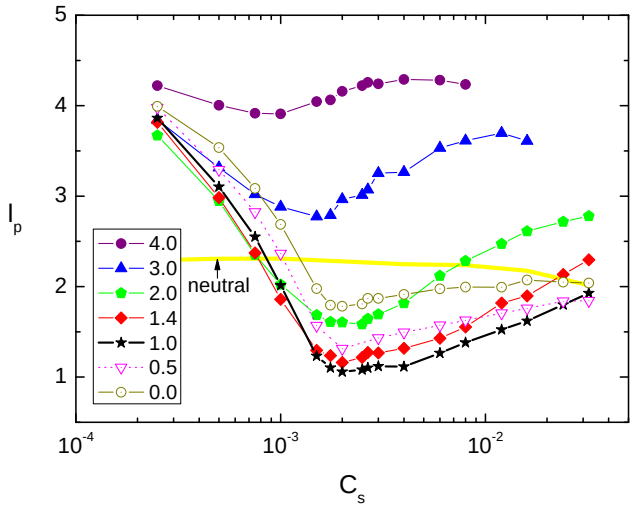

FIG. 6: $\ell_{\rm p}$ as a function of $C_{\rm s}$ for different σ_{+4}. The symbol used for each σ_{+4} is indicated at the left-bottom side of the figure. The error bars are smaller than the size of the symbols. The bare persistence length ℓ_0 is depicted as reference and marked by "neutral".

in the chain collapse region and increases in the chain reexpansion region. A minimum value appears in the vicinity of $C_{\rm s}^*$. The degree of increase diminishes with decreasing σ_{+4}. For vanishing σ_{+4}, it is so weak that $\ell_{\rm p}$ is roughly a constant as $C_{\rm s} > C_{\rm s}^*$. Similar to the results in the previous sections, $\ell_{\rm p}$ increases with both increasing and decreasing σ_{+4} from 1.0. $\sigma_{+4} = 1.0$, therefore, denotes a condition to separate the two behaviors of evolution of $\ell_{\rm p}$.

The persistence length has generally two contributions: the bare persistence length ℓ_0 (in the absence of electrostatic force) and the electrostatic persistence length $\ell_{\rm e}$ (owing to the Coulomb interaction) [35, 36]. In this study, the bare persistence length ℓ_0 was calculated by performing simulations on the referenced system where four neutral chains and 192 neutral particles are placed in salt solutions. The result is depicted in Fig. 6 and the curve is marked

by "neutral". We found that ℓ_0 is not sensitive to the salt concentration and roughly attains a value 2.3. It slightly decreases in the high-salt region, probably due to the jamming effect by the salt ions. For the polyelectrolyte solutions with large σ_{+4} ($\sigma_{+4} = 3.0$ and 4.0), the $\ell_{\rm p}$ curve thoroughly lies above the ℓ_0 curve, indicating a more rigid flexibility than a neutral polymer. The electrostatic persistence length is, hence, positive. On the other hand, for the polyelectrolyte solutions with $\sigma_{+4} \leq 2.0$, $\ell_{\rm p}$ is smaller than ℓ_0 in the mid-salt region and shows one or two intersections with the ℓ_0 curve. Therefore, $\ell_{\rm e} = \ell_{\rm p} - \ell_0$ is positive in a salt-free solution and becomes eventually negative upon addition of salt. It increases in the high-salt region and reattains a positive value for $\sigma_{+4} = 1.4$ or 2.0.

The negative contribution of electrostatics to the persistence length has been experimentally observed [39, 40]. Recently Ariel and Andelman (AA) pointed out that a negative $\ell_{\rm e}$ indicates a mechanical instability (collapse) of polyelectrolytes due to the presence of multivalent counterions [48]. By taking into account the thermal fluctuations and correlations between bound counterions, they derived an expression of $\ell_{\rm e}$ for an intrinsically-rigid charged polymer in (Z:1)-salt solutions in the limit of $b \ll \kappa^{-1} \ll (N-1)b$:

$$\ell_{\rm e} = \left(\Gamma(2-\Gamma) - \frac{(\Gamma-1)^2}{\Gamma \ln(\kappa b)} \right) \ell_{\rm e}^{\rm OSF} \tag{10}$$

where $\Gamma = Z\ell_{\rm B}/b$ is the Coulomb strength parameter between a monomer and a Z-valent counterion, $\kappa = \sqrt{4\pi Z(Z+1)\ell_{\rm B} C_{\rm s}}$ is the inverse Debye-Hückel screening length, and $\ell_{\rm e}^{\rm OSF} = (4Z^2\kappa^2\ell_{\rm B})^{-1}$ is the electrostatic persistence length deduced by Odijk-Skolnick-Fixman (OSF) theory [35, 36]. In the derivation, they have assumed point-like charges for the ions. We present, in Fig. 7, $\ell_{\rm e}$ obtained from the simulations and that predicted by Eq. (10) as a function of κ. We witnessed that $\ell_{\rm e}$ depends strongly on the size of the tetravalent ions. The negative regime of $\ell_{\rm e}$ has been successfully captured in the simulations. To make a comparison with the theoretical prediction, we focused on the case with vanishing σ_{+4}. Please notice that this case does not exactly fulfill the assumption of the theory because in the simulations, the monovalent counterions and coions are not point charge-like and, also, the chains are not rigid. However, according to our experiences [25], ions other than multivalent counterions do not play a decisive role on the properties of polyelectrolytes. This comparison, therefore, makes sense if the effect of chain rigidness is negligible. We emphasize that the electrostatic correlations are fully taken into account in the simulations. In our study, the region in which Eq. (10) is valid is $0.02 \ll \kappa \ll 0.91$ because $Z = 4$, $\ell_{\rm B} = 3$,

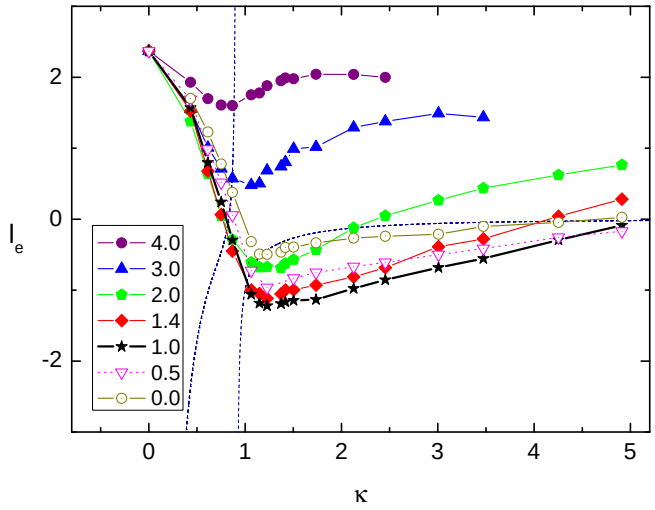

FIG. 7: ℓ_e as a function of κ for different σ_{+4}. The symbol used for each σ_{+4} is indicated at the left-bottom side of the figure. The error bars are smaller than the size of the symbols. The dashed curve depicts ℓ_e predicted by Eq. (10).

and b is about 1.1. Notice that Eq. (10) has a singularity at $\kappa = 1/b \simeq 0.91$ and, hence, the curve is divided into two branches. The left branch is located in the valid region but fails to predict ℓ_e. It gives not only a wrong value but also a wrong trend of variation of ℓ_e against κ. We noticed that Eq. (10) is a modification of $\ell_e^{\rm OSF}$ multiplied by a factor but the valid region given by AA theory [48] is incompatible with that of OSF theory. OSF theory is held when the screening length κ^{-1} is much smaller than the bare persistence length [44]. Therefore, AA theory may be true in the region $\kappa \gg 1/b$. As shown in the figure, ℓ_e for vanishing σ_{+4} is well described by the right branch of the curve of Eq. (10), which seems to support this conjecture. This topic deserves a further analysis in the future.

E. Potential of mean force

Experiments and simulations have shown that like-charged macroions can attract each other in a solution [66–68]. It is hence relevant to know under which conditions the like-charge attraction takes place between polyelectrolytes. To answer this question, we investigate "potential of mean force" in this section. Potential of mean force describes the effective interaction between two particles (molecules) in a medium, which includes two contributions: the direct interaction between two particles (molecules) and the indirect interaction

via other particles (molecules) and the medium. This quantity can be calculated by simulations: $W_{\alpha\beta}(r) = -k_{\rm B}T \ln g_{\alpha\beta}(r)$ where $g_{\alpha\beta}(r)$ is the radial distribution function between particles of species α and β. $g_{\alpha\beta}(r)$ is computed by

$$g_{\alpha\beta}(r) = \frac{V\langle H_{\alpha\beta}(r)\rangle}{N_\alpha N_\beta (4\pi r^2 \delta r)} \tag{11}$$

where N_α and N_β are the number of α-particles and that of β-particles, respectively, V is the volume of the simulation box, and $H_{\alpha\beta}(r) = \sum_{i=1}^{N_\alpha} h_{i\beta}(r)$ with $h_{i\beta}(r)$ denoting the number of β-particles lying in a spherical shell, centered at the α-particle i, of radius r and shell thickness δr.

Because our system is composed of only four chains, it is not easy to reduce statistical error if we directly calculate the potential of mean force between chains. We, therefore, calculated the potential of mean force between monomers on different chains, which also provides the information about the chain interaction. We denote this quantity $W_{\rm mm'}(r)$ and the results are presented in Fig. 8 which contains six plots, from top to bottom and from left to right, corresponding, in orders, to the cases $\sigma_{+4} = 0.0$, 0.5, 1.0, 2.0, 3.0 and 4.0. $W_{\rm mm'}(r)$ for the referenced neutral polymers is also depicted in the figure. In a salt-free solution, $W_{\rm mm'}(r)$ displays a repulsive interaction, and is stronger than that for the neutral polymers owing to the electrostatic repulsion between monomers. This can be seen by comparing the range of repulsion estimated by equaling $W_{\rm mm'}(r)$ to the thermal energy $k_{\rm B}T$. The range of repulsion is at $r = 7.1$ for the polyelectrolytes and at $r = 3.0$ for the neutral polymers. Upon addition of salt, $W_{\rm mm'}(r)$ responses in two distinct ways, which depends on the ion size. The first one is applied for small or large tetravalent counterions, such as $\sigma_{+4} = 0.0$, 0.5, or 4.0. In these cases, $W_{\rm mm'}(r)$ is purely repulsive in the course of addition of salt. Hence, the monomers on different chains repel between themselves and the system exhibits no like-charge attraction. The second way is happened for an intermediate size such as $\sigma_{+4} = 1.0$, 2.0, or 3.0. At this moment, $W_{\rm mm'}(r)$ displays an attractive well in a mid-salt region. Therefore, it appears like-charge attraction between chains. In the first case, the range of repulsion of $W_{\rm mm'}(r)$ decreases to a minimum value nearly at $C_{\rm s} = 0.002$. Further increase of $C_{\rm s}$ either leaves $W_{\rm mm'}(r)$ unchanged (for vanishing σ_{+4} and for $\sigma_{+4} = 4.0$) or increases the range of repulsion of $W_{\rm mm'}(r)$ (for $\sigma_{+4} = 0.5$). We will call $W_{\rm mm'}(r)$ at $C_{\rm s} = 0.002$ "the curve at equivalence", which separates two behaviors of evolution of $W_{\rm mm'}(r)$ as $C_{\rm s}$ is increased or decreased from $C_{\rm s}^*$. We noticed that $W_{\rm mm'}(r)$ tends toward the referenced curve of the neutral polymers at

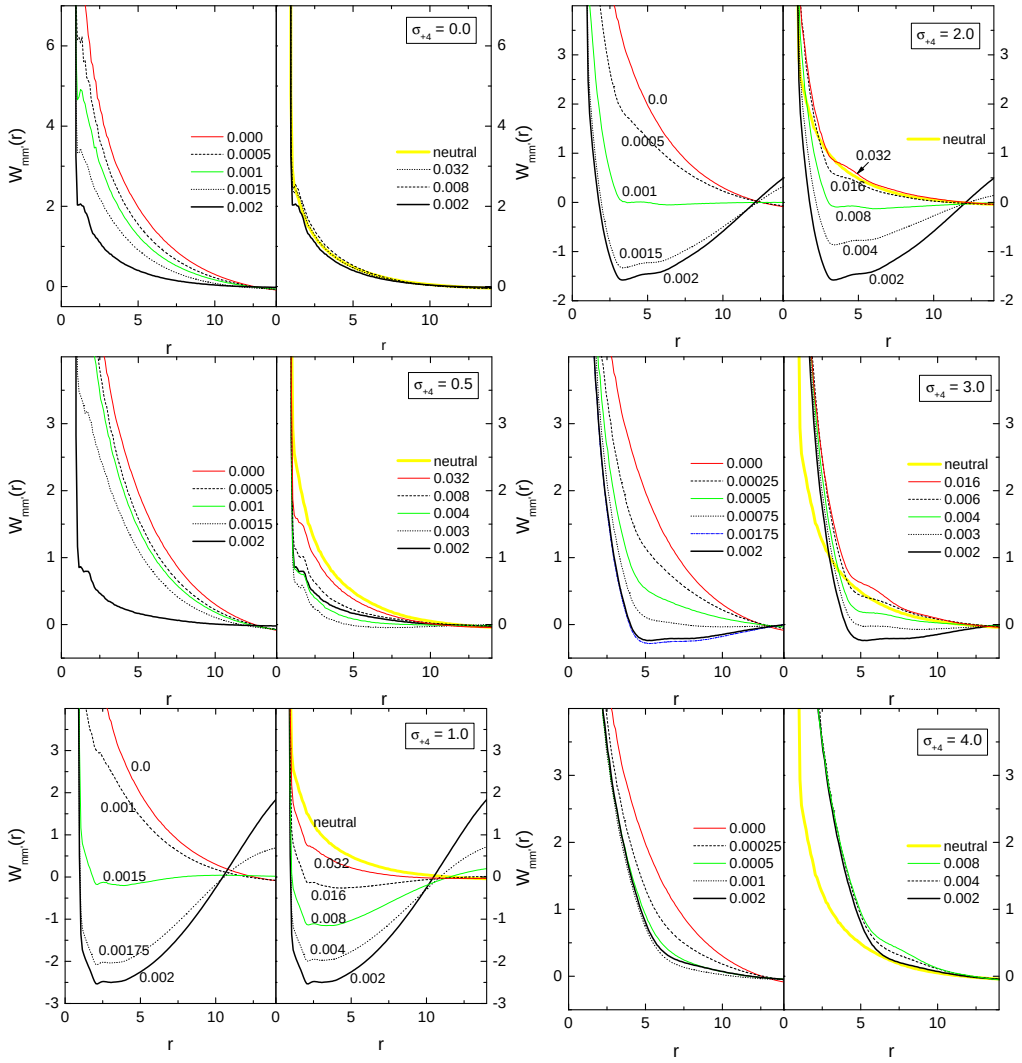

FIG. 8: $W_{\mathrm{mm}'}(r)$ for $\sigma_{+4} = 0.0$, 0.5, 1.0, 2.0, 3.0 and 4.0, shown, in orders, from top to bottom and from left to right, in six plots. Each plot includes several $W_{\mathrm{mm}'}(r)$ at different C_{s}. The value of C_{s} is indicated in the plot or near the corresponding curve. $W_{\mathrm{mm}'}(r)$ for the neutral polymer system is depicted as reference and marked by "neutral". The unit of ordinate axis is $k_{\mathrm{B}}T$.

high salt concentrations except for the deviation happened at small r due to the excluded volume of large ions. For vanishing σ_{+4}, the curve at equivalence is very close to the reference curve and $W_{\mathrm{mm}'}(r)$ is roughly unchanged while $C_{\mathrm{s}} > 0.002$. For $\sigma_{+4} = 0.5$, the curve at equivalence lies below the referenced curve; $W_{\mathrm{mm}'}(r)$ is bounded between the two curves and increases with C_{s}. And in the second case, $W_{\mathrm{mm}'}(r)$ displays a potential well located near $r = \sigma_{\mathrm{m}} + \sigma_{+4}$. It suggests an attraction mediated by a tetravalent counterion. The depth of the well can be more profound than $k_{\mathrm{B}}T$. Therefore, a stable bound state can be

formed between monomers on different chains and it is a prerequisite to occur salt-induced phase separation. The maximum depth of the well is happened while $C_{\rm s}$ is $C_{\rm s}^*$. In general, we found that $W_{\rm mm'}(r)$ is bounded between the salt-free curve and the curve at equivalence while $C_{\rm s} < 0.002$, and between the latter curve and the referenced neutral curve while $C_{\rm s} > 0.002$.

We have shown that the occurrence of the like-charge attraction depends on both salt concentration and ion size. In Fig. 9 we present, in the variable space, the region where $W_{\rm mm'}(r)$ shows an attractive well. In the figure, the data points (symbolized by star) denote

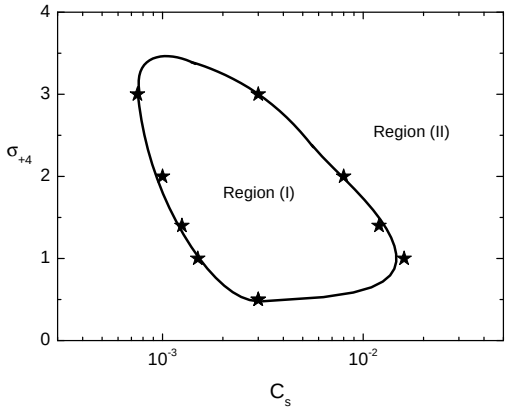

FIG. 9: Two distinct regions in the ($C_{\rm s}$, σ_{+4})-variable space. In Region (I), $W_{\rm mm'}(r)$ shows an attractive well and in Region (II), it is purely repulsive.

the salt concentrations for a given σ_{+4}, at which a purely repulsive $W_{\rm mm'}(r)$ turns to show an attractive well and *vice versa*, and the closed solid curve is sketched to help readers to separate the two regions. It clearly shows that an effective attraction appears only when σ_{+4} is neither too small nor too big and salt concentration is intermediate around the equivalence concentration. We mention that the occurrence of an attractive region in the potential of mean force is not sufficient to have a phase separation of the system. Phase transitions in charged colloid systems have been largely discussed in literatures but there have been relatively few studies of phase transitions in charged chain systems (see Refs. [69] and [70] and references therein).

Fig. 10 shows snapshots of the simulations for $\sigma_{+4} = 0.5$, 1.0 and 4.0 at two salt concentrations $C_{\rm s} = 0.002$ and $C_{\rm s} = 0.008$. At $C_{\rm s} = 0.002$, we saw that the polyelectrolytes favor to be apart from each other for both of the cases $\sigma_{+4} = 0.5$ and $\sigma_{+4} = 4.0$. However, delicate difference was witnessed that the previous case displays a single-chain collapse but the latter

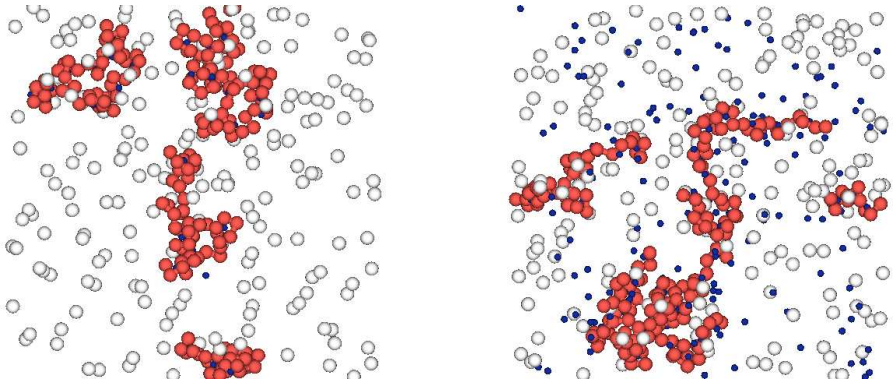

(a)

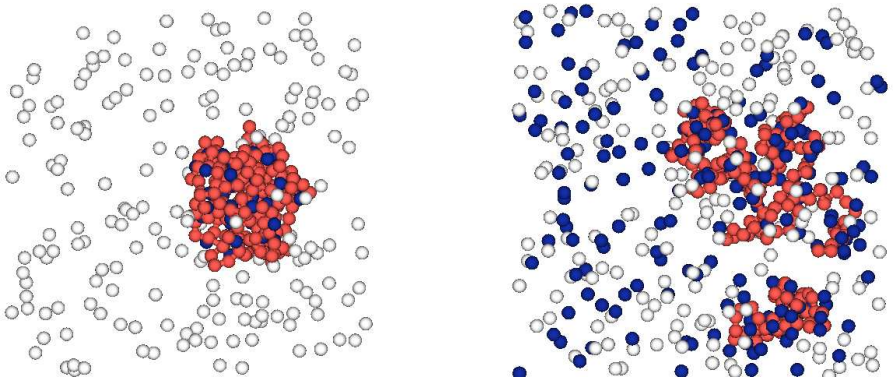

(b)

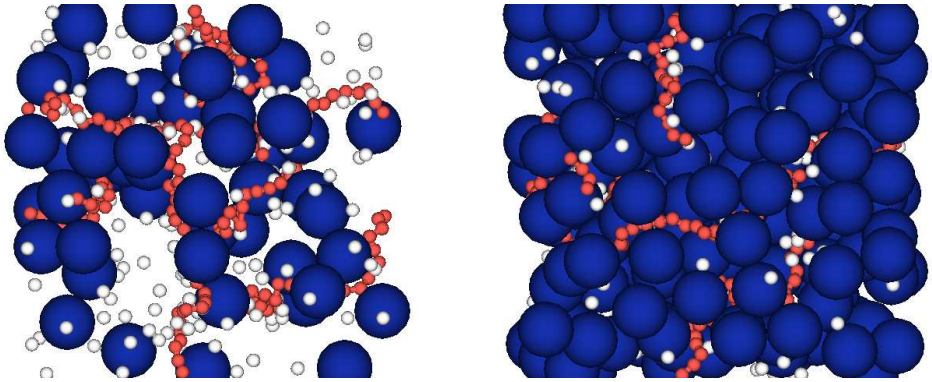

(c)

FIG. 10: (Color online) Snapshots of simulations for (a) $\sigma_{+4} = 0.5$, (b) $\sigma_{+4} = 1.0$, and (c) $\sigma_{+4} = 4.0$, at $C_s = 0.002$ (left) and $C_s = 0.008$ (right). In the pictures, the bead-spring chains are represented in gray color (red color online) and the monovalent counterions in light one (white color online). The tetravalent counterions are represented in dark-colored (blue-colored online) particles whereas the coions are not plotted for the clarity of the pictures. In the snapshots, a chain may appear more than one fragment because of periodic boundary condition.

one does not. For $\sigma_{+4} = 1.0$, the chains favor to aggregate together, in accordance with the results of Fig. 8 which show the occurrence of an attraction between the negatively-charged polymers. This attraction is mediated by counterions, mainly the tetravalent counterions, since almost all the tetravalent counterions are condensed on the polyelectrolytes. We point out that the condensation of tetravalent counterion is not a sufficient condition to occur chain aggregation. It can be seen from the case $\sigma_{+4} = 0.5$ in which most of the tetravalent counterions are condensed but the chains does not aggregate. At the high salt concentration $C_{\rm s} = 0.008$, the attraction between chains is reduced, in comparison with the cases at $C_{\rm s} = 0.002$. The chains segregate or show tendency of segregation from each other. In the simulations, we observed that while $C_{\rm s} > 0.002$, only part of the tetravalent counterions can condense onto the chains.

F. Integrated charge distribution around a chain

In this section, we investigate the charge distribution around a polyelectrolyte. It enables to understand how ions distribute around a chain and provides useful information for theorists to develop models. We define a worm-like tube of radius r around a chain to be a union of N spheres of radius r centered at each monomer on the chain. We calculated the averaged total charge inside a worm-like tube, including the charge of the ions and the one of the monomers. This quantity is called "the integrated charge distribution" and is denoted by $Q(r)$.

We show in Fig. 11 $Q(r)$ at various $C_{\rm s}$ for σ_{+4} ranged between 0.0 and 4.0. Focus firstly on the case with vanishing σ_{+4}. In the region $r < 0.5$, $Q(r)$ attains a value equal to the bare charge of a chain, -48. A stair-like behavior then appears for $Q(r)$ in the region $0.5 < r < 1.0$ while $0.0 < C_{\rm s} < 0.002$. Outside the region, $Q(r)$ monotonically increases and tends toward zero at large r due to electroneutrality. Since $r < 1.0$ is the depletion zone for the particles other than tetravalent counterions, the behavior of $Q(r)$ in this region is completely determined by the condensation of tetravalent counterions. The stair-like behavior indicates a *perfect* condensation on the surface of the chain, owing to the vanishing size of the tetravalent counterions. For instance, at $C_{\rm s} = 0.001$, we have 24 tetravalent counterions in the simulation box and, therefore, 6 condensed tetravalent counterions on a chain, in average. A perfect condensation will lead to a value -24 for $Q(r)$ and this is

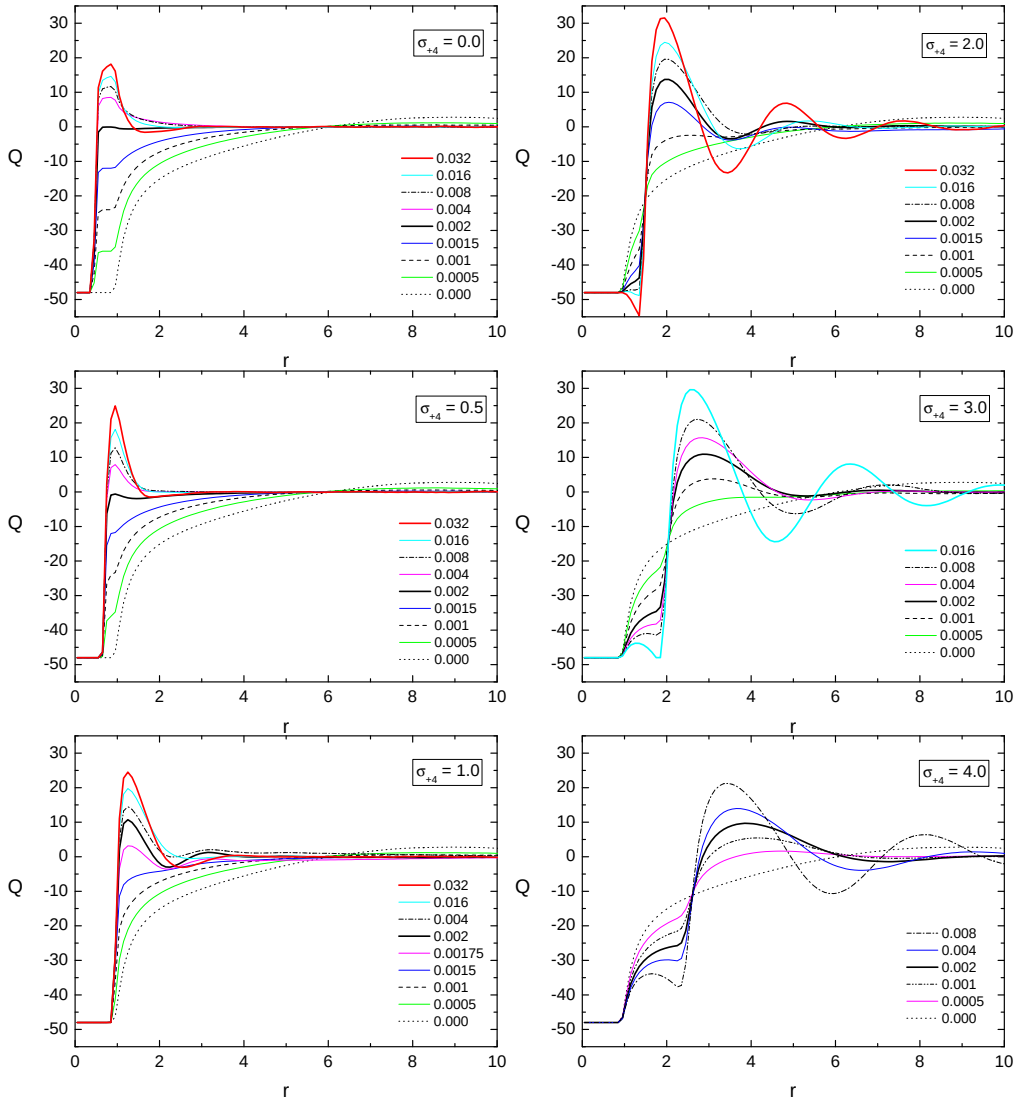

FIG. 11: $Q(r)$ at different C_s for σ_{+4}=0.0, 0.5, 1.0, 2.0, 3.0 and 4.0, shown, in orders, from top to bottom and from left to right, in six figures. The line arts used for different C_s are indicated at the right-bottom side of each figure.

exactly what we have observed in the figure. At the equivalence concentration, $Q(r)$ is zero while $r > 0.5$. If C_s is further increased ($C_s > 0.002$), $Q(r)$ reveals a positive peak in the region $0.5 < r < 1.0$, which indicates an overcharging, and, then, rapidly decays to zero as $r > 1.0$. The hight of the peak suggests that only a portion of the tetravalent counterions are condensed on the chain. For the case $\sigma_{+4} = 0.5$, the region in which only the tetravalent counterions can intervene is narrowed to $0.75 < r < 1.0$. In the region, the step of the stair-like $Q(r)$ becomes tilted while $C_s < 0.002$. If $C_s > 0.002$, $Q(r)$ displays a positive

peak, which is more pronounced than that for vanishing σ_{+4}. For the case $\sigma_{+4} = 1.0$, an oscillatory behavior occurs at high C_s. Similar phenomena have been observed in other systems such as charged plate [71], colloid system [72], and rigid polyelectrolyte [23]. This oscillatory behavior indicates a multi-layer organization of ions: in the close neighborhood of a polyelectrolyte, tetravalent counterions condense and form a positively-charged layer which overcharges the chain; exterior to this layer, anionic particles intervene and form a negatively-charged layer which overcompensates the charge inside and, hence, the integrated charge becomes negative, and so forth. Notice that the depletion zone around a chain for tetravalent counterions is $r < (1 + \sigma_{+4})/2$. It becomes larger than that for the other ions while $\sigma_{+4} > 1.0$. In these cases, $Q(r)$ decreases with increasing C_s in the depletion zone, but shows completely opposed behavior just outside the zone apparently due to the condensation of tetravalent counterions. At very high C_s (for instance, at $C_s = 0.032$ for $\sigma_{+4} = 2.0$), $Q(r)$ in the zone can even attain a value smaller than the chain bare charge. In this case, negative particles are the major composition of the first ion layer around a chain, which is counterintuitive. The following three observations are worth to be noticed. (1) The salt concentration at which $Q(r)$ becomes (roughly) zero in the region $r > (1+\sigma_{+4})/2$ decreases with increasing σ_{+4}. (2) The oscillatory behavior appears more markedly for large σ_{+4} than for small one. (3) At a given C_s, the larger the σ_{+4}, the higher the maximum peak of $Q(r)$ will be.

It is tempting to consider that a polyelectrolyte and the ions condensed on the chain form a complex object. Under some conditions, the effective charge of the complex object reverses its sign. This phenomenon is called charge inversion [49]. Nguyen *et al.* intended to link the phenomenon of charge inversion with the reentrant condensation [5]. They proposed that zero effective charge and charge inversion of chains are, respectively, the cause for the condensation and for the redissolution of polyelectrolytes. Their theory necessitates further verification either by experiments or by simulations. In the rest of this section, we try to calculate the effective charge of a polyelectrolyte, in hope of being able to clarify the relationship between the charge inversion and the reentrant condensation. We simply define the complex to be the set of particles lying within a worm-like tube of radius r_c around the chain. This definition has been utilized in many places, for example, in Refs. [18] and [73]. Usually, r_c is chosen to be the distance at which the electrostatic attraction between a monovalent counterion and a monomer is equal to the kinetic energy $\frac{3}{2}k_BT$; in consequence,

the counterion inside the tube of radius r_c can not escape from the chain. We, thus, consider the total charge $Q(r_c)$ inside the tube as the effective charge of a chain. In our study, r_c is equal to 2. The results are presented in Fig. 12(a). Two behaviors were observed: (1) for

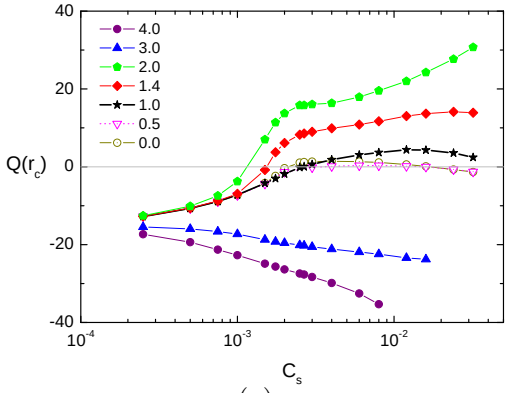

(a)

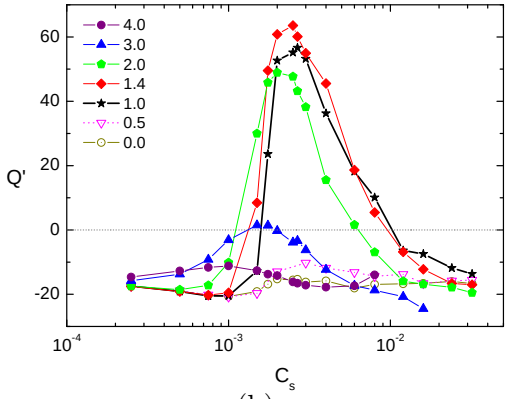

(b)

FIG. 12: (a) $Q(r_c)$ as a function of $C_{\rm s}$ with $r_c = 2.0$, and (b) Q' as a function of $C_{\rm s}$, for different σ_{+4}. The symbol used to denote each σ_{+4} is indicated in the figures.

$\sigma_{+4} = 3.0$ and 4.0, $Q(r_c)$ decreases with increasing $C_{\rm s}$, (2) for $\sigma_{+4} \leq 2.0$, $Q(r_c)$ increases basically with $C_{\rm s}$. Notice that $Q(r_c)$ for $\sigma_{+4} = 1.4$ or 2.0 attains a large positive value in the mid-salt region. Hence, $W_{\rm mm'}(r)$ should show strong repulsion in this region, according to the theory of Nguyen *et al.* But, in fact, we observed a strong attractive well for $W_{\rm mm'}(r)$ and the chains were observed to aggregate together. Therefore, the results do not support the theory.

We notice that it is too simple to regard $Q(r_c)$ as the effective chain charge, because ion valence is not considered in the definition. For example, the suitable r_c for tetravalent counterions should be 8.0, based upon the same argument to choice r_c for monovalent coun-

terions. In addition, $r_c = 2.0$ becomes too small while $\sigma_{+4} \geq 3.0$, since the depletion zone around a chain for the tetravalent counterions is bigger than the tube. Therefore, we redefine $r_c = 8.0$ as the novel condensation region for tetravalent counterions, whereas keeping $r_c = 2.0$ for monovalent counterions and for monomers on the other chains. Considering that the condensation of coions is mainly mediated by tetravalent counterions, we choose $r_c = 8.0$ for coions. The charges inside the different tubs are computed and their sum Q' is then regarded as an alternative definition for the effective chain charge. The results are presented in Fig. 12(b). We remark that Q' looks quite differently from $Q(r_c)$. It shows a positive peak in the mid-salt region for $\sigma_{+4} = 1.0$, 1.4, and 2.0 but retains negative value for the other σ_{+4}. The obtained results suggest a disconnection between neutralization of chain charge and condensation of polyelectrolytes.

Our simulating system in the high-salt region reveals a picture more close to the one described by Solis [52]: although *locally* overcompensated by condensed counterions, the net charge of a redissolved chain can be positive or negative due to the association of coions. We must point out that the effective chain charge interpreted by $Q(r_c)$ or by Q' in this section can be only served as a reference because both $Q(r_c)$ and Q' are sensitive to the choice of r_c. A rigorous way to study it, which can circumvent the ambiguity, is to study the electrophoretic mobility of polyelectrolytes in salt solutions. This part of research is currently undergoing.

IV. CONCLUSIONS

We have performed molecular dynamics simulations in canonical ensemble to investigate the properties of highly-charged polyelectrolytes in tetravalent salt solutions, including chain morphology, single-chain structure factor, swelling exponent, persistence length, like-charge attraction between chains and integrated charge distribution around a polyelectrolyte. We have explored a wide range of salt concentration and studied the effect of size of tetravalent counterions on the above properties.

We have found that a polyelectrolyte exhibits, in turns, two conformational transitions upon addition of salt: a collapsed transition and a reexpanding transition, manifested by a V-shaped curve of the square of radius of gyration $\langle R_{\rm g}^2 \rangle$ against salt concentration $C_{\rm s}$. The systems at different monomer concentration $C_{\rm m}$ show similar curves. The curves overlap

each other in the chain-reexpansion region. In the chain-collapsed region, we have also observed that $A_{\rm m}(\langle R_{\rm g}^2\rangle - \langle R_{\rm g}^{*2}\rangle)$ against $C_{\rm s}/C_{\rm m}$ lie over each other for different $C_{\rm m}$, where $A_{\rm m}$ and $\langle R_{\rm g}^{*2}\rangle$ weakly depends on $C_{\rm m}$. These findings are useful in understanding the phase boundaries of the condensation of polyelectrolytes: on the upper boundary, $C_{\rm s}$ is roughly independent of $C_{\rm m}$ and on the lower one, $C_{\rm s}$ depends linearly on $C_{\rm m}$.

The study of chain morphology shows that for the cases with σ_{+4} (the size of the tetravalent counterions) around 1.0, the chains reveal compact and prolate structures in the vicinity of the equivalence concentration $C_{\rm s}^*$. In a low-salt region and in a high-salt region, the chains show extended structures. At a very high salt concentration, the chains behave similarly to neutral polymers. For the cases with large σ_{+4}, the chains are elongated and do not display a collapsed-transition in the mid-salt region. For the case with vanishing σ_{+4}, the behavior of the chains is analogous to that of neutral polymers as $C_{\rm s} > C_{\rm s}^*$. Noticeably, our results show that $\sigma_{+4} = 1.0$ is the optimal condition to pack polyelectrolytes into the smallest volume.

We have shown that the single-chain structure factor $S(q)$ of the multi-chain system in salt solutions follows the Guinier function $N(1 - q^2\langle R_{\rm g}^2\rangle/3)$ while $q \ll R_{\rm g}^{-1}$. $S(q)$ then exhibits a power-law-like behavior q^s in the region $R_{\rm g}^{-1} \ll q \ll \sigma_{\rm m}^{-1}$, suggesting that the scaling law, $R_{\rm g} \sim N^{\nu}$, is held for polyelectrolytes in salt solutions. The swelling exponent $\nu = -1/s$ attains a minimum value near $C_{\rm s}^*$ and behaves in analogy of the morphological quantities. It shows once more that the chains are mostly collapsed while σ_{+4} is compatible with 1.0.

Our simulations incorporated explicitly the salt ions and, therefore, were able to study the negative regime of the electrostatic persistence length $\ell_{\rm e}$. This regime appears simultaneously with the mechanical instability of the polyelectrolytes induced by salt. We have examined the theory of Ariel and Andelman [48] and found that it fails to predict $\ell_{\rm e}$ in the *so-claimed* valid region $b \ll \kappa^{-1} \ll (N-1)b$ but describes $\ell_{\rm e}$ well in the unexpected region $\kappa^{-1} \ll b$. Since the OSF theory is valid in the latter region, we conjectured that the theory of Ariel and Andelman is applicable in the latter region. This part deserves a detail investigation in the future.

We have studied like-charge attraction between polyelectrolytes by calculating the potential of mean force $W_{\rm mm'}(r)$ between monomers on different chains. The results show that it depends strongly on salt concentration and ion size. An attractive region appears in $W_{\rm mm'}(r)$ only when the salt concentration is intermediate and the tetravalent counterions possess a

size compatible with the monomers. The most profound attractive well is happened while $\sigma_{+4} = 1.0$ and $C_s = C_s^*$.

In the final part, the integrated charge distribution $Q(r)$ around a polyelectrolyte was investigated. We have found that the chain charge can be locally overcompensated by condensed ions. $Q(r)$ displays an oscillatory behavior at high salt concentrations while $\sigma_{+4} \geq 1.0$. The oscillatory behavior results from a multi-layer organization of ions around the chain, which is in agreement with the picture predicted by Solis [52]. We have used two different definitions to calculate the effective chain charge. The results suggest that charge inversion is not a necessary condition to occur reentrant condensation. Recently Wen and Tang have provided evidence against the connection between charge inversion and resolubilization of polyelectrolyte bundles [74]. A more rigorous study by electrophoresis performed by molecular dynamics simulations is undergoing.

V. ACKNOWLEDGMENTS

The author acknowledges C.-L. Lee, Y.-F. Wei, and N. Pardillos for their comments. This material is based upon work supported by the National Science Council, the Republic of China, under the contract No. NSC 94-2112-M-007-023. Most of the simulations were running at the National Center for High-performance Computing. The author expresses his gratitude to the members and the staffs of the council and the center.

---

[1] H. G. Bungenberg de Jong and J. Lens, Bioch. Z. **235**, 185 (1931).

[2] A. Ikegami and N. Imai, J. Polym. Sci. **56**, 133 (1962).

[3] M. Olvera de la Cruz, L. Belloni, M. Delsanti, J. P. Dalbiez, O. Spalla, and M. Drifford, J. Chem. Phys. **103**, 5781 (1995).

[4] E. Raspaud, M. Olvera de la Cruz, J.-L. Sikorav, and F. Livolant, Biophys. J. **74**, 381 (1998).

[5] T. T. Nguyen, I. Rouzina, and B. I. Shklovskii, J. Chem. Phys. **112**, 2562 (2000).

[6] V. A. Bloomfield, Curr. Opin. Struct. Biol. **6**, 334 (1996).

[7] V. Vijayanathan, T. Thomas, and T. J. Thomas, Biochem. **41**, 14085 (2002).

[8] H. R. Kruyt, ed., *Colloid Science*, vol. II (Elsevier Publishing Company, New York, 1949).

[9] M. Saminathan, T. Antony, A. Shirahata, L. H. Sigal, T. Thomas, and T. J. Thomas, Biochem. **38**, 3821 (1999).

[10] S. K. Tripathy, J. Kumar, and H. S. Nalwa, eds., *Handbook of Polyelectrolytes and Their Applications*, vol. I, II, III (American Scientific, Stevenson Ranch, CA, 2002).

[11] M. J. Stevens, Phys. Rev. Lett. **82**, 101 (1999).

[12] M. J. Stevens, Biophys. J. **80**, 130 (2001).

[13] R. Chang and A. Yethiraj, J. Chem. Phys. **118**, 11315 (2003).

[14] M. J. Stevens and K. Kremer, J. Chem. Phys. **103**, 1669 (1995).

[15] R. G. Winkler, M. Gold, and P. Reineker, Phys. Rev. Lett. **80**, 3731 (1998).

[16] S. Liu and M. Muthukumar, J. Chem. Phys. **116**, 9975 (2002).

[17] M. J. Stevens and S. J. Plimpton, Eur. Phys. J. B **2**, 341 (1998).

[18] S. Liu, K. Ghosh, and M. Muthukumar, J. Chem. Phys. **119**, 1813 (2003).

[19] J. Kłos and T. Pakula, J. Chem. Phys. **122**, 134908 (2005).

[20] M. O. Khan and D. Y. C. Chan, Macromolecules **38**, 3017 (2005).

[21] R. S. Dias, A. A. C. C. Pais, and M. G. Miguel, J. Chem. Phys. **119**, 8150 (2003).

[22] J. M. G. Sarraguça, M. Skepo, A. A. C. C. Pais, and P. Linse, J. Chem. Phys. **119**, 12621 (2003).

[23] M. Deserno and C. Holm, Mol. Phys. **100**, 2941 (2002).

[24] E. Allahyarov, H. Löwen, and G. Gompper, Europhys. Lett. **68**, 894 (2004).

[25] P.-Y. Hsiao, J. Chem. Phys. **124**, 044904 (2006).

[26] M. Muthukumar, J. Chem. Phys. **86**, 7230 (1987).

[27] M. Muthukumar, J. Chem. Phys. **105**, 5183 (1996).

[28] G. A. Christos and S. L. Carnie, J. Chem. Phys. **91**, 439 (1989).

[29] P.-G. de Gennes, *Scaling Concepts in Polymer Physics* (Cornell U.P., Ithaca, N.Y., 1979).

[30] C. Peterson, O. Sommelius, and B. Söderberg, J. Chem. Phys. **105**, 5233 (1996).

[31] H. Schiessel and P. Pincus, Macromolecules **31**, 7953 (1998).

[32] H. Schiessel, Macromolecules **32**, 5673 (1999).

[33] Q. Liao, A. V. Dobrynin, and M. Rubinstein, Macromolecules **36**, 3386 (2003).

[34] N. Bjerrum, K. Dan. Vidensk. Selsk. Math. Fys. Medd. **7**, 9 (1926).

[35] T. Odijk, J. Polym. Sci. Part B: Polym. Phys. **15**, 477 (1977).

[36] J. Skolnick and M. Fixman, Macromolecules **10**, 944 (1977).

[37] M. Le Bret, J. Chem. Phys. **76**, 6243 (1982).

[38] M. Fixman, J. Chem. Phys. **76**, 6346 (1982).

[39] C. G. Baumann, S. B. Smith, V. A. Bloomfield, and C. Bustamante, Proc. Natl. Acad. Sci. USA **94**, 6185 (1997).

[40] T. Hugel, M. Grosholz, H. Clausen-Schaumann, A. Pfau, H. Gaub, and M. Seitz, Macromolecules **34**, 1039 (2001).

[41] U. Micka and K. Kremer, Phys. Rev. E **54**, 2653 (1996).

[42] M. Ullner, B. Jönsson, C. Peterson, O. Sommelius, and B. Söderberg, J. Chem. Phys. **107**, 1279 (1997).

[43] T. T. Nguyen and B. I. Shklovskii, Phys. Rev. E **66**, 021801 (2002).

[44] R. Everaers, A. Milchev, and V. Yamakov, Eur. Phys. J. E **8**, 3 (2002).

[45] M. Ullner, J. Phys. Chem. B **107**, 8097 (2003).

[46] L. Guldbrand, B. Jönsson, H. Wennerström, and P. Linse, J. Chem. Phys. **80**, 2221 (1984).

[47] M. J. Stevens, M. L. Falk, and M. O. Robbins, J. Chem. Phys. **104**, 5209 (1996).

[48] G. Ariel and D. Andelman, Phys. Rev. E **67**, 011805 (2003).

[49] A. Y. Grosberg, T. T. Nguyen, and B. I. Shklovskii, Rev. Mod. Phys. **74**, 329 (2002).

[50] F. J. Solis and M. Olvera de la Cruz, J. Chem. Phys. **112**, 2030 (2000).

[51] F. J. Solis and M. Olvera de la Cruz, Eur. Phys. J. E **4**, 143 (2001).

[52] F. J. Solis, J. Chem. Phys. **117**, 9009 (2002).

[53] M. P. Allen and D. J. Tildesley, *Computer Simulation of Liquids* (Oxford University Press, New York, 1987).

[54] B. Dünweg and K. Kremer, Phys. Rev. Lett. **66**, 2996 (1991).

[55] E. Dubois and F. Boué, Macromolecules **34**, 3684 (2001).

[56] Z. Ou and M. Muthukumar, J. Chem. Phys. **123**, 074905 (2005).

[57] Y. Oono and M. Kohmoto, J. Chem. Phys. **78**, 520 (1983).

[58] M. Rubinstein and R. H. Colby, *Polymer Physics* (Oxford University Press, 2003).

[59] B. Dünweg, D. Reith, M. Steinhauser, and K. Kremer, J. Chem. Phys. **117**, 914 (2002).

[60] K. Šolc, J. Chem. Phys. **55**, 335 (1971).

[61] M. Bishop and C. J. Saltiel, J. Chem. Phys. **88**, 6594 (1988).

[62] O. Jagodzinski, E. Eisenriegler, and K. Kremer, J. Phys. I (France) **2**, 2243 (1992).

[63] M. Müller, K. Binder, and L. Schäfer, Macromolecules **33**, 4568 (2000).

[64] P.-Y. Hsiao and E. Luijten, submitted (2006).

[65] M. Ullner and C. E. Woodward, Macromolecules **35**, 1437 (2002).

[66] W. M. Gelbart, R. F. Bruinsma, P. A. Pincus, and V. A. Parsegian, Physics Today **53**, 38 (September 2000).

[67] T. E. Angelini, H. Liang, W. Wriggers, and G. C. L. Wong, Proc. Natl. Acad. Sci. USA **100**, 8634 (2003).

[68] F. Molnar and J. Rieger, Langmuir **21**, 786 (2005).

[69] P. Taboada-Serrano, C.-J. Chin, S. Yiacoumi, and C. Tsouris, Curr. Opin. Colloid Interface Sci. **10**, 123 (2005).

[70] A. Z. Panagiotopoulos, J. Phys.: Condens. Matter **17**, S3205 (2005).

[71] H. Greberg and R. Kjellander, J. Chem. Phys. **108**, 2940 (1998).

[72] R. Messina, E. González-Tovar, M. Lozada-Cassou, and C. Holm, Europhys. Lett. **60**, 383 (2002).

[73] R. R. Netz, J. Phys. Chem. B **107**, 8208 (2003).

[74] Q. Wen and J. X. Tang, J. Chem. Phys. **121**, 12666 (2004).

[75] This work was performed using molecular dynamics simulator LAMMPS. For more information about LAMMPS, refer to http://www.cs.sandia.gov/∼sjplimp/lammps.html.

[76] The average bond length in our simulations is about 1.1 σ_{m}.